HHS Public Access

Author manuscript

Biomed Microdevices. Author manuscript; available in PMC 2015 July 02.

Published in final edited form as:

Biomed Microdevices. 2015 February ; 17(1): 24. doi:10.1007/s10544-014-9909-6.

Impedance characterization, degradation, and *in vitro* biocompatibility for platinum electrodes on BioMEMS

Thomas Geninatti,
Houston Methodist Research Institute (HMRI), 6670 Bertner Avenue, Houston, TX 77030, USA. University of Chinese Academy of Science (UCAS), Shijingshan, 19 Yuquan Road, Beijing 100049, China

Giacomo Bruno,
Houston Methodist Research Institute (HMRI), 6670 Bertner Avenue, Houston, TX 77030, USA. Politecnico di Torino, Corso Duca degli Abruzzi 24, Turin 10129, Italy

Bernardo Barile,
Houston Methodist Research Institute (HMRI), 6670 Bertner Avenue, Houston, TX 77030, USA. Politecnico di Torino, Corso Duca degli Abruzzi 24, Turin 10129, Italy

R. Lyle Hood,
Houston Methodist Research Institute (HMRI), 6670 Bertner Avenue, Houston, TX 77030, USA

Marco Farina,
Houston Methodist Research Institute (HMRI), 6670 Bertner Avenue, Houston, TX 77030, USA

Jeffrey Schmulen,
Houston Methodist Research Institute (HMRI), 6670 Bertner Avenue, Houston, TX 77030, USA

Giancarlo Canavese, and
IIT - Italian Institute of Technology, Center for Space Human Robotics, Corso Trento 21, Tutin 10129, Italy. Department of Applied Science and Technology, Politecnico di Torino, Lungo Piazza d'Armi 6, Chivasso 10034, Italy

Alessandro Grattoni
Houston Methodist Research Institute (HMRI), 6670 Bertner Avenue, Houston, TX 77030, USA

Alessandro Grattoni: agrattoni@houstonmethodist.org

Abstract

Fine control of molecular transport through microfluidic systems can be obtained by modulation of an applied electrical field across channels with the use of electrodes. In BioMEMS designed for biological fluids and *in vivo* applications, electrodes must be biocompatible, biorobust and stable. In this work, the analysis and characterization of platinum (Pt) electrodes integrated on silicon substrates for biomedical applications are presented. Electrodes were incorporated on the surface of silicon chips by adhesion of laminated Pt foils or deposited at 30°, 45° or 90° angle by e-beam or physical vapor (sputtering) methods. Electrical and physical properties of the electrodes were

Correspondence to: Alessandro Grattoni, agrattoni@houstonmethodist.org.

Thomas Geninatti and Giacomo Bruno contributed equally to this work.

quantified and evaluated using electrical impedance spectroscopy and modelling of the electrode-electrolyte interfaces. Electrode degradation in saline solution at pH 7.4 was tested at room temperature and under accelerated conditions (90 °C), both in the presence and absence of an applied electrical potential. Degradation was quantified using atomic force microscopy (AFM) and inductively coupled plasma mass spectroscopy (ICP-MS). Biocompatibility was assessed by MTT proliferation assay with human dermal fibroblasts. Results demonstrated that the deposited electrodes were biocompatible with negligible material degradation and exhibited electrochemical behavior similar to Pt foils, especially for e-beam deposited electrodes. Finally, Pt electrodes e-beam deposited on silicon nanofabricated nanochannel membranes were evaluated for controlled drug delivery applications. By tuning a low applied electrical potential (<1.5 VDC) to the electrodes, temporal modulation of the dendritic fullerene 1 (DF-1) release from a source reservoir was successfully achieved as a proof of concept, highlighting the potential of deposited electrodes in biomedical applications.

Keywords

Implantable electrodes; E-beam deposition; Sputter deposition; Nanochannel membranes; Drug delivery

1 Introduction

Controlled and selective transport of analytes through nanochannel membranes has been broadly demonstrated by tuning electrophoresis (Fine et al. 2011), electroosmotic flow (Yeh et al. 2012) electrostatic gating (Grattoni et al. 2011a, b) and ionic concentration polarization (Yossifon et al. 2009) through generation of an electrical potential across channels. This control is relevant to a broad spectrum of biomedical applications, including drug delivery (Desai et al. 1999; Ferrati et al. 2013, In press; Celia et al. 2014), molecular sieving (Fu et al. 2007), cell sorting (Gossett et al. 2010), and cell transplantation (Desai et al. 1998; Sabek et al. 2013). In drug delivery, the ability to fine tune release profiles for specific therapeutic agents is highly beneficial in personalized treatments requiring dose titration or synchronization with the biological clock, the fundamental principle in chronotherapy (Smolensky and Peppas 2007; Youan 2010).

Our research group has developed an implantable silicon membrane for constant, long-term release of therapeutics (Walczak et al. 2005). This platform has been specifically designed for hormone replacement, organ transplantation, and cancer prevention, among others (Fine et al. 2010; Ferrati et al. 2013, In press; Sih et al. 2013). We hypothesized that drug release through our membrane could be modulated by using a low-voltage electrical potentials. To accomplish this, it was necessary to develop a suitable strategy for creating biorobust electrodes with long-term biocompatibility and stability on the surface of prefabricated membranes. The primary challenge stemmed from whether thin platinum (Pt) films could be integrated with our implantable membrane technology without compromising the functionality of the system or occluding the micro- and nanoscale fluidic architecture. Pt was selected as the material of choice as it is highly biocompatible, biorobust, and highly conductive.

In this study, three different approaches for creating Pt electrodes were investigated and compared: electron beam (e-beam) deposition, physical vapor deposition (CVD) (sputtering), and direct adhesion of laminated Pt foil. Pt foils were considered the standard for comparison in terms of bioinertness and electrochemical properties. However, despite their intrinsic simplicity, foils are expensive and difficult to adapt to an intricate fluidic structure (Han et al. 2003). In contrast, e-beam and sputter deposition are inexpensive, flexible approaches allowing for precise control of electrode thicknesses, even on complex surfaces (Vieu et al. 2000). Functional differences in these techniques include the sputtering method's advantage in reproducibility and high film density while e-beam deposition achieves higher placement accuracy (Döring et al. 1997). However, a potential limitation of these approaches is poor adhesion of Pt to the substrate, which requires the adoption of surface-specific adhesion layers (de Haro et al. 2002) and may be affected by the angle of deposition. Analyses were performed using three different angle of deposition with respect to the substrate surface (30°, 45° and 90°) for both e-beam- and sputter- coating. In many instances, as is the case for our membranes, an angle of deposition lower than 90° is required to avoid occluding channels or pores, which are directly accessible onto by deposited species, being perpendicular to the device surface. However, a small angle of deposition may cause higher porosity, reduced homogeneity, and poor adhesion of the deposited film, affecting the electrochemical performances and robustness of the electrode. For the electrochemical analysis of the electrodes, silicon chips coated by SiN and reproducing the same surface chemistry as our nanochannel membranes where used as the substrate. A SiO_2 – Ti adhesion layer was added to promote adhesion. Electrodes were characterized in terms of electrical behavior, degradation, and biocompatibility. Electrical behavior was evaluated through electrical impedance spectroscopy (EIS). Franks' model of electrode-electrolyte interface (Franks et al. 2005) was employed to quantify the parameters of electrical capacity, leakage resistance, and surface roughness. Electrochemical characterization in cell culture was performed to determinate variation in electrical properties over a 3-day period. Protein adsorption was evaluated by attenuated total reflectance Fourier transform infrared spectroscopy (ATR-FTIR). Atomic force microscopy (AFM) and inductively coupled plasma mass spectroscopy (ICP-MS) were utilized to quantify degradation. Biocompatibility was assessed by measuring cell viability through an MTT assay. Finally, as proof-of-concept, Pt electrodes were e-beam deposited onto our silicon nanochannel membranes and the tunable release of dendritic fullerene 1 (DF-1) was tested in response to an applied electrical potential.

2 Materials and methods

2.1 Sample fabrication

Silicon wafers (700 μm thick) were coated by chemical vapor deposition (CVD) with a 1.7 μm SiN film (Novellus Concept II Sequel, AZ). Three separate methods were employed to integrate the electrodes on the chip surface: i) electron beam (e-beam) deposition of a Pt film, ii) sputter deposition of a Pt coat, and iii) laminated Pt foil. For i) and ii), a SiO_2 (250 nm) substrate was deposited on the SiN surface in the presence of argon plasma to ensure a defect-free dielectric layer. Then, a Ti adhesion layer was formed prior to the final Pt film. Ti (10 nm) and Pt (60 nm) layers were obtained at three different angles of deposition with

respect to the substrate surface (30°, 45° and 90°) achieving equal layer thicknesses perpendicular to the substrate. For iii) Pt foils (100 μm thickness) were obtained from Sigma Aldrich (Sigma Aldrich, St. Louis, MO, USA) and laser-cut (A-Laser, Inc., CA, USA) to a 6 mm×6 mm square shape.

2.2 Electrical characterization

Wafers were diced into 10 mm×10 mm chips. Insulated 36 AWG conductors were epoxied to the electrodes (H20E, Epoxy Technology, MA) and cured at 130 °C for 15 min. A lead free solder (SN99, MG Chemicals, BC, Canada) was used to wire Pt foils electrodes. Electrodes/wafer sandwiches were fabricated from all the electrodes types (Fig. 1). For deposited electrodes, the Si surfaces of two chips were bonded with a non-conductive epoxy (J-B Kwik, J-B Weld, TX), leaving the two Pt sides facing outward. The laser-cut foil electrodes were assembled onto the two sides of silicon chips using a double-adhesive Teflon tape (CS Hyde Company, IL). Sandwiches were immersed in PBS (pH 7.4) at room temperature (RT). Electrodes characterization was performed by electrical impedance spectroscopy (EIS) with 3 replicate sandwiches for each electrode type. A 1.5 V_{pp} sine wave was applied with a function/arbitrary wave generator (33522A, Agilent Technologies, CA) at frequency steps in the range of 1 Hz to 10 kHz. An oscilloscope (U2702A, Agilent Technologies) was used in series to the sandwich and in parallel to a 100Ω shunt resistor. The oscilloscope was communicated through MATLAB® software for the data acquisition and analysis. Ten measurements were collected at each frequency step. Fast Fourier Transform (FFT) was used to remove the environment interference. Finally, processed data were averaged.

2.3 The model

Frank's model was used for the comparative analysis of electrochemical impedance between foil laminated and deposited Pt electrodes, see Fig. 2 (Franks et al. 2005). The model describes the interface between the metal electrode and electrolytes. According to Franks, the interface was modelled as a parallel system between the leakage resistance (or transfer resistance), R_t, and the constant phase element $Z(f)=1/(i2\pi fQ)^n$, where f is the frequency, Q is the electrode capacity, and n represents the surface irregularities (related to the roughness) of electrodes ($0 \leq n \leq 1$ where 1 stands for the ideally smooth surface). The electrolyte is modelled by ohmic impedance, R_a, in series with the metal interface. The electrode capacity is a function of its surface area, which is intrinsically linked to the roughness parameter n. By analyzing Q and n is therefore possible to define the extent of degradation of the electrode. The leakage parameter R_t describes the tendency of the electrodes to be converted into ions at the interface metal/fluid. The model was fitted to the experimental data through MATLAB® software ($R^2>0.99$). The model parameters were obtained by minimizing the aberrance from the average impedance spectrum by the nonlinear least square method and the trust-region algorithm.

The breaking frequency, f_{LF}, considered as the borderline between the low frequencies (LF) and the medium frequency (MF), was calculated from the parameters obtained by Frank's model as:

$$f_{LF} = \frac{1}{2\pi Q \sqrt[n]{R_t}} \quad (1)$$

The transition between the high frequency (HF) and MF domain was defined corresponding to $R_a/R_t = 10$. The high frequency cutoff point, f_{HF}, was calculated as follows:

$$f_{HF} = \frac{\sqrt[n]{\frac{10R_t - R_a}{R_t R_a}}}{2\pi Q} \quad (2)$$

2.4 Electrical characterization in cell culture

Human adult dermal fibroblasts PCS-201-012 (ATCC, Manassas, VA, USA) were seeded into 12-well plates (10, 000 cells/well in 3 ml medium) using ATCC® Primary Cell Solution Fibroblast Growth Kit-Low Serum (ATCC® PCS-201-041) added to Fibroblast Basal Medium (ATCC® PCS-201-030). The culture was left to adhere overnight at 37 °C in incubator with 5 % CO_2. The wired chip sandwiches (Fig. 1) employed in the previous electrical characterization were sterilized in ethanol, rinsed in sterile PBS, and housed in the 12-well plate. EIS analysis was performed as previously detailed with the time points at 1, 5, 10, 24, 48 and 65 h. The parameters R_t, R_a, Q, and n were determined for each timepoint.

2.5 ATR-FTIR spectroscopy

Pt electrodes sputtered at 30°, 45°, and 90° were immersed in a protein-rich environment to determine the protein adsorption on their surfaces. The chips were cleaned by submersion in IPA for 1 h and drying with nitrogen gas. Electrodes were immersed in 3 ml of either MilliQ water (n=3) or ATCC Fibroblast Basal Medium (ATCC PCS-201-030) (n=3) for 72 h, for each deposition angle. Samples were rinsed with MilliQ water, dried with nitrogen gas. ATR-FTIR was used to evaluate the protein adsorption on Pt electrodes. Spectra analysis was conducted with a Nicolet 6700 FTIR spectrometer (Thermo Fisher Scientific, Waltham, MA, USA), within the 500–4000 cm^{-1} spectral range at 4 cm^{-1} resolution. Interferograms were averaged for 128 scans. The spectra were interactively baselined and normalized at 3725 cm^{-1} with SigmaPlot software.

2.6 Degradation

Twenty-four wired chip sandwiches (Fig. 1) were tested for degradation without an applied potential (n=12) or an applied 1.5 VDC voltage (n=12) by means of a stabilized power supply (E3643A, Agilent Technologies). Chips were immersed in 10 ml of PBS (Sigma-Aldrich, MO, USA) contained within a borosilicate glass bottle and kept either at RT or under accelerated degradation conditions (90 °C). The test was performed for 20 days with three replicate chips for each set of experimental conditions. At days 1, 10, and 20, the surface roughness (R_{RMS}) was measured by AFM (BioScope Catalyst, Bruker, MA, USA). Samples of the hosting PBS solution were collected at days 10 and 20 to quantify the amount of degraded Pt by ICP-MS (720-ES, Varian, CA, USA). Statistical relevance of differences among groups were evaluated through t-test (α=0.05).

2.7 Biocompatibility

Human adult dermal fibroblasts PCS-201-012 (ATCC) were seeded into 12-well plates (10,000 cells/well in 3 ml medium) and left to adhere overnight in the same media conditions described above. E-beam deposited (90°) wired sandwich chips (Fig. 1) were housed in cell culture inserts (BD Falcon, NJ, USA) and immersed in the 12-well plates. Either 0 VDC (n=3) or 1.5 VDC (n=3) were applied to the chips through a power supply (E3643A, Agilent Technologies). Cells were incubated with chips for 24, 48, and 72 h. Cells incubated in absence of chips were used as a negative control. Cell proliferation was checked at 24, 48, and 72 h by adding 3 ml of 3-(4,5-dimethylthiazol-2-yl)-2,5-diphenyltetrazolium bromide solution (MTT reagent, Sigma) at a concentration of 0.5 mg/ml into each well. Cells were incubated with MTT reagent for 1 h, after which the solution was replaced with 3 ml of dimethyl sulfoxide. Following a 15 min incubation period at RT, the UV absorbance of the supernatant was measured at 590 nm with a Synergy H4 plate reader (BioTek, VT, USA).

2.8 Testing electrodeposition Pt electrodes on silicon membrane

A Si-SiN membrane for drug delivery (NanoMedical Systems, Inc., Austin, TX) with 200 nm nanochannels was coated with the SiO_2-Ti-Pt electrode stack as previously detailed. To avoid channel clogging, the deposition was performed at an angle~45° with respect to the membrane surface. Membranes were wired as described above, wet with isopropyl alcohol, rinsed in DI water, and housed in a custom dual chamber diffusion testing device (Grattoni et al. 2011a, b). The source reservoir of the device was loaded with 150 μl of a 3 mg/ml solution of DF-1 in 50 mM NaCl. The sink reservoir, provided by a UV-cuvette, was loaded with 4.45 ml of 50 mM NaCl in DI water. The device was housed in a custom robotic carousel (Geninatti et al. 2014) interfaced with a UV–vis spectrophotometer (Cary 50, Agilent Technologies). Electrical potentials were applied to the membrane electrodes by means of a DC power supply (E3643A, Agilent Technologies) as follows: 0 VDC for 15 min, +1.5 VDC for 60 min, 0 VDC for 60 min, −1.5 VDC for 60 min and 0 VDC for 60 min. UVabsorption (λ=320 nm) of the sink solution was automatically collected at a frequency of 1 Hz over 255 mins.

3 Results and discussion

3.1 Electrical characterization in PBS

Electrical characterization was performed to evaluate the impedance of e-beam and sputter deposited Pt electrodes in comparison to laminated Pt foils. The EIS data were evaluated with the Franks model, a non-linear model chosen to account for the behaviors at low-frequencies, which differentiates it from other established models (Franks et al. 2005). The model parameters were calculated at a 95 % confidence by fitting experimental data to the model over a frequency range from 1 to 10 kHz. These results are listed in Table 1. Analysis to 10 kHz was considered sufficient as impedance for all electrodes reached a plateau after 5–8 kHz. Investigation at frequencies lower than 1 Hz was not performed due to signal-to-noise limitations. The stability of the R_a parameter was used to validate individual experiments, as the impedance provided by the electrolyte solution should be highly conserved between tests. Small variations within the 10 % range are present for all

electrodes with the exception of the Pt foils due to the different soldering methods. Electrodes sputtered at 45° and e-beam deposited at 90° exhibited the highest impedance values at low frequencies. Analogous values were obtained for the R_t determined for Pt foils and the 30° and 90° sputtered electrodes, while deposition at the same angle by the e-beam method resulted in significantly lower impedance values, causing redox reactions to be accelerated. A comparison of roughness measurements (n) showed that 30° e-beam and 45° sputter deposited electrodes had the smoothest surfaces (0.72 and 0.73, respectively), while all other samples (Pt foils included) gave similar values in the range 0.5 to 0.6. The capacity (Q) of the deposited electrodes exceeded the capacity of the Pt foils by one to two orders of magnitude (with the exception of the 45° e-beam electrode). One explanation lies with the differences in manufacturing protocol between the deposited and laminated electrodes generated discrepancies in the total surface area.

The cutoff frequencies, f_{LF} and f_{HF} (Eqs. 1 and 2, respectively), delineate the LF, MF, and HF domains. At HF, the deposited electrodes behaved similarly to the Pt foils, where R_a is predominant. Since the contribution of the constant phase element (Q) is equal in all frequency equations, the variation of this parameter shifts the domain demarcation equally for both the high and low frequency cutoffs (Eqs. 1 and 2). Considering Q as constant, it is possible to define the f_{LF} and f_{HF} as primarily functions of R_t in the LF domain and R_a in the HF domain, assuming $R_t \gg R_a$ and identical roughness. Hence, the entire system can be approximated by considering the impedance at these two frequencies. At LF (<1 mHz) all the electrodes behave similarly to the Pt foils, despite constant impedance. This indicates the electrodes could potentially be employed within constant current devices such as micropumps (Nguyen and Kassegne 2008) or MEMS electrostatic actuators (Mukundan and Pruitt 2009). Looking at Fig. 3a–b, the HF domain (>4 kHz) is characterized by a plateau where all electrodes converge to a similar R_a resistance. At MF, similar behavior is observed for the 30° and 90° sputter deposited and 90° e-beam deposited electrodes, as is evident by their nearly parallel slopes in Fig. 3a–b.

3.2 Electrical characterization in cell culture

Figure 3c shows the behavior of electrodes in cell culture (human adult dermal fibroblasts) at 37 °C over a period of 65 hrs. Figure 3c shows the transition between f_{LF} and f_{HF} for all deposited electrodes, with the exception of the 30° e-beam deposition as it proved unstable (evident due to variability of the R_a measured). The top graph in Fig. 3c describes a homogeneous increase in this frequency over time, which is most apparent for the 45° e-beam and the 90° sputtered electrodes. Minor growths in frequency are presented by all other samples with the exception of the 30° sputtered electrode due to the aforementioned instability in leak resistance. In Fig. 3c, the bottom chart describes more stable behavior in the high frequency domain, as all electrodes maintain their values within the same order of magnitude over the spectrum. This is proven by the strict correlation between degradation of the electrodes and the surface exposed to the cell medium. Minor differences in frequency are observed in the sputtered samples, suggesting that 48 h are required for the electrodes to reach a stable electrochemical conformation. Figure 3d shows the variation of R_a and R_t over time, characterizing the HF and the LF impedance. No significant variation was observed for the R_a parameters, confirming the stability of the cell culture media and validating the

results. Consequently, these electrodes may prove similar in electrical behavior to the Pt foils in the LF and HF regimes once constant impedance is considered. The 30° sputtered electrodes are the major exception, showing a constant increase of R_t over time. This increase may be ascribed to the adhesion of protein on the electrode surfaces.

3.3 ATR-FTIR analysis

When a biomaterial is implanted in a living body, adsorption of blood and interstitial protein usually occurs, quickly creating a film on an implant's exposed surfaces (Zhang et al. 1998). This phenomenon might influence the effective impedance of surface deposited electrodes, and determining the plausibility of this event is necessary for understanding the long-term *in situ* behavior of our implants. Chittur demonstrated that ATR-FTIR is highly sensitive and provides valuable insight on surface protein adsorption (Chittur 1998). Spectral data analyzed in the range from 800 to 2000 cm^{-1} are shown in Fig. 4. Pt electrodes submerged in MilliQ water, and used as a negative control, presented a flat spectra, attributed to the lack of protein on the sample surfaces. Results from Pt electrodes immersed in cell culture media showed a spectrum identifying protein adsorption, especially in the range 1400 to 1000 cm^{-1} assigned to radical chains of proteins, and 1720 cm^{-1} to 1495 cm^{-1} assigned to amides region (composed by amide I and II) that represents the main backbone vibration modes of protein (Taraballi et al. 2010). The highest protein adsorption was observed in the 90° Pt sputtered electrodes, followed by 30° and 45° depositions angles. ATR-FTIR analysis confirmed the adsorption of protein on the electrode surfaces, providing a potential explanation for increasing R_t values over time.

3.4 Degradation

Characterizing electrode degradation of the deposited metal is of primary importance as the manufacturing process utilized may compromise device performance and be harmful to the biological environment. We tested degradation by AFM and ICP-MS. The results are shown in Fig. 5 and values tabulated in Tables 2 and 3. It has to be noted that the R_{RMS} values obtained by AFM are closely related to the scanned area and number of data points (Russell et al. 2004). Some fluctuations in value are therefore linked to the difficulty in accurately locating and scanning the same 5 μm×5 μm sections of the electrode surface at each time point. To achieve a statistically relevant analysis, mean and standard deviation values shown in Fig. 5 were obtained from 12 (Fig. 5a) or 36 (Fig. 5b) measurements each. In general, regardless of the angle of deposition, e-beam produced smoother surfaces than sputtering with average values equal to 1.5±0.7 nm and 3.3±2.0 nm, respectively. Interestingly, increased average R_{RMS} was observed at increasing deposition angle for e-beam (0.9±0.4 nm at 30°, 1.5±0.5 nm at 45°, 2.1±0.5 nm at 90°), while decreasing values were obtained for sputtering (4.4±2.6 nm at 30°, 3.1±1.2 nm at 45°, 2.2±1.3 nm at 90°). We are unsure of the reason for these opposing trends, but speculate they may be attributable to the higher impact energy of particles deposited through sputtering. By averaging data obtained at 23 °C and 90 °C and 0 VDC and 1.5 VDC applied potential, no major variations were observed over time for e-beam data (Fig. 5a), indicating in first degree inertness of the electrode surface. However, in the case of sputtered electrodes, a statistically relevant decrease in R_{RMS} was observed between day 1 and day 10 of immersion in PBS. This could be due to a rapid smoothing of the most prominent surface irregularities obtained by sputtering. The

application of 1.5 VDC did not produce any significant change in the surface R_{RMS} for both e-beam and sputtered electrodes (Fig. 5b). This result was expected, as the applied potential is below the threshold of charge injection occurs for Pt (2 VDC) (Burke and Ivory 2008; Cogan 2008). An exception is represented by the e-beam 30° electrode where a significant increase in R_{RMS} was observed in response to the applied potential. Layering could occur by depositing Pt by e-beam at a steep angle. A delamination of thin Pt layers from the chip could occur at the application of an electrical potential. Finally, data shows that for most deposition angles for both e-beam and sputtered electrodes, accelerated degradation conditions (90 °C) caused a general increase in R_{RMS} with respect of 23 °C samples (in average 24 and 57 %, respectively) (Fig. 5c). This result was expected as degradation phenomena are directly dependent on the internal energy of the system. As shown in Table 2, R_{RMS} values remained within an acceptable range (<9 nm), confirming that the electrode surfaces remained smooth and effect of degradation minor. Data demonstrate that even under the worst degradation conditions (1.5 V, 90 °C), the R_{RMS} did not change dramatically and overt surface alteration was not observed. AFM data were confirmed by the results of ICP-MS, which showed a negligible amount of Pt degraded from the electrodes. The amount of Pt degraded in solution per unit of surface area (Table 3) did not show a clear trend with time on either passive (0 V) and active (1.5 V) tests. As expected, the most severe degradation occurred, for most of the samples, under accelerated conditions (90 °C) and applied electrical potential.

3.5 Biocompatibility

For potential *in vivo* drug delivery applications, our Pt electrode would be encased in a biocompatible reservoir prior to being implanted subcutaneously. The electrode would therefore be in close proximity to, but not in direct contact with, the surrounding tissues. To study the electrode-cells interactions simulating this implantation scenario *in vitro*, electrodes were immersed in cell culture medium and dermal fibroblasts were grown in close proximity. Dermal fibroblasts were chosen as a cell type relevant to the envisioned implant location for this platform. The viability of the cells was tested by means of an MTT assay at time points 24, 48, and 72 h. The data (Fig. 6) showed negligible difference in proliferation rates between cells grown in the presence of electrodes, both powered and quiescent, and the untreated controls (without electrodes). These results are in agreement with similar *in vitro* and *in vivo* studies reported in the literature which show normal cell proliferation of fibroblasts grown on Pt substrates (Turner et al. 2004; Sevcencu et al. 2007; Pennisi et al. 2009). Thus, MTT results provided here are preliminary indications of these electrodes' biocompatibility.

3.6 Evaluation of electrodeposited electrodes on Si-SiN membrane

Based on our results, we selected 45° e-beam deposition method as the ideal approach to fabricate Pt electrodes on the surfaces of our pre-microfabricated, 200 nm nanochannel membranes (see Fig. 7a). This choice was based on the 45° deposition angle having the desired combination of stability, robustness, and electrochemical properties at DC. By tuning an electrical potential with the electrodes in the range of −1.5 VDC to +1.5 VDC, electrophoretic control of DF-1 (net charge −10.4 at pH 7.4) was achieved (Fig. 7b). Specifically, application of a 1.5 VDC electrical potential with the cathode at the sink-side

electrode caused complete interruption of DF-1 release. Subsequent deactivation of the applied potential resulted in a return to normal, passive, concentration-driven release. When applying 1.5 VDC with reverse bias (anode at the sink-side), a dramatic increase in release rate (approximately 100 % with respect of passive release) was observed. Transitory behavior was observed for 15 min following each potential modulation prior to the release profile reaching a steady state. This period was consistent with the time required for homogenization of the sink fluid after abrupt changes in release rate.

These results indicate that electrodes can be incorporated through e-beam deposition on pre-fabricated nanochannel devices without causing channel occlusion. Further, it serves as a proof-of-concept that such electrodes could be adopted for fine tuning the release of charged analytes and drug molecules with respect to implantable drug delivery applications.

3.7 Additional discussion

The experimental results described above offer significant insight relevant to any biomedical microdevice utilizing metal electrodes, an increasingly common occurrence with the widespread development and propagation of lab-on-a-chip and other BioMEMS (Stieglitz and Gross 2002; Cheung and Renaud 2006). Continued progression and acceptance of these systems will require methods for producing reliable and inexpensive electrodes, motivating adaptation of flexible approaches developed for microelectronic fabrication such as e-beam and sputter deposition (Vieu et al. 2000). The utility of the findings related here may be better understood through analysis of electrode parameters within the three delineated frequency domains (HF, MF, LF). In the HF domain (>4 kHz), the electrode's capacitance contribution is negligible, allowing the resistance of the electrolytic solution to be predominant. This suggests that, to a certain extent, geometric alterations to Pt electrodes employed in applications within the HF domain will have negligible effect, potentially allowing electrodes used as mass filters for mass spectrometers (Cheung et al. 2010), redox capacitors (Sun et al. 2010), and pudendal nerve efferent axion stimulators (Tai et al. 2004) to be shaped as necessary. In the MF domain (1 mHz<MF<4 kHz), the surface area and the R_{RMS} are the primary contributors to the slope of the Bode plot, suggesting that 30° and 90° sputtered electrodes would be more suitable for applications such as retina (Humayun et al. 1999) and carotid stimulators (Tordoir et al. 2007). In the LF (<1 MHz), R_t is the primary determinant of electrode impedance. This enables preferential electrode selection for LF applications, such as the nDS platform developed by this group. The R_t data suggest the most suitable Pt electrodes for our application are the 90° and 45° e-beam depositions. The latter is less likely to clog our nanochannels, and is therefore the better choice. Similar analysis can be used to choose electrodes for other devices operating in the defined LF domain, such as pacemakers or spinal cord stimulators (Alo et al. 1998).

4 Conclusions

In this study, Pt electrodes were fabricated on silicon chips through e-beam and sputter deposition at 30°, 45° and 90° with respect to the chip surface. Electrodes were characterized for electrical impedance through EIS in PBS and cell culture, degradation by AFM and ICP-MS, and *in vitro* biocompatibility through an MTT assay with human fibroblast cells. Data were compared to the results achieved with standard laminated Pt

electrodes. Electrical characterization showed that all electrode configurations had similar electrochemical properties at frequencies lower than 1 mHz or higher than 4 kHz, defining a bandwidth conventionally used in biomedical applications. An ATR-FTIR test provided confirmation of protein adsorption on electrodes, a finding consistent with EIS measurements in cell culture. Degradation tests performed with and without an applied potential of 1.5 VDC showed that electrodes maintained high chemical inertness and surface integrity at both RT and 90 °C, even in cell culture. The MTT proliferation assay exhibited negligible differences between cells incubated in the proximity of electrodes or controls, even when a 1.5 VDC potential was applied. Comparative analysis of these results suggested the most suitable electrode fabrication method for LF applications, such as the nDS, are 90° and 45° e-beam depositions. Further, the latter is less likely to cause obstruction of the nanochannels, indicating it to be the most appropriate electrode manufacturing technique. As a proof-of-concept, a pre-microfabricated implantable silicon membrane was modified through e-beam deposition of a Pt electrode at a 45° and demonstrated successful temporal modulation of DF-1 release through an applied electrical potential. These studies provide preliminary evidence on the suitability of e-beam and sputtered Pt thin films as biocompatible and biorobust electrodes that can be conveniently integrated onto other pre-fabricated devices for biomedical applications (Grattoni et al. 2010; Fine et al. 2013). In the case of controlled drug delivery, these agile, flexible, and inexpensive deposition methods represent promising approaches for the successful development of actively tunable implantable delivery devices.

Acknowledgments

The authors are grateful to Silvia Ferrati, Eugenia Nicolov, Francesca Taraballi, and Eszter Vörös for help in the manuscript finalization. NanoMedical Systems, Inc. (Austin, TX) provided the silicon membrane. This work was supported with funds from CASIS (GA-14-145), Houston Methodist Hospital Research Institute and NIH NIGMS R21 GM 111544.

References

Alo KM, Yland MJ, Kramer DL, Charnov JH, Redko V. Neuromodulation. 1998; 1(1):30–45. [PubMed: 22150884]

Burke JM, Ivory CF. Electrophoresis. 2008; 29(5):1013–1025. [PubMed: 18306183]

Celia C, Ferrati S, Bansal S, van de Ven AL, Ruozi B, Zabre E, Hosali S, Paolino D, Sarpietro MG, Fine D, Fresta M, Ferrari M, Grattoni A. Adv Healthc Mater. 2014; 3(2):230–238. [PubMed: 23881575]

Cheung KC, Renaud P. Solid State Electron. 2006; 50(4):551–557.

Cheung, K.; Velasquez-Garcia, LF.; Akinwande, AI. Micro Electro Mechanical Systems (MEMS), 2010 I.E. 23rd International Conference on; 2010. p. 867-870.

Chittur KK. Biomaterials. 1998; 19(4–5):357–369. [PubMed: 9677150]

Cogan SF. Annu Rev Biomed Eng. 2008; 10:275–309. [PubMed: 18429704]

de Haro C, Mas R, Abadal G, Munoz J, Perez-Murano F, Dominguez C. Biomaterials. 2002; 23(23): 4515–4521. [PubMed: 12322971]

Desai TA, Chu WH, Tu JK, Beattie GM, Hayek A, Ferrari M. Biotechnol Bioeng. 1998; 57(1):118–120. [PubMed: 10099185]

Desai T, Hansford D, Kulinsky L, Nashat A, Rasi G, Tu J, Wang Y, Zhang M, Ferrari M. Biomed Microdevices. 1999; 2(1):11–40.

Döring S, Birke P, Weppner W. Ionics. 1997; 3(3–4):184–193.

Ferrati S, Fine D, You J, De Rosa E, Hudson L, Zabre E, Hosali S, Zhang L, Hickman C, Sunder Bansal S, Cordero-Reyes AM, Geninatti T, Sih J, Goodall R, Palapattu G, Kloc M, Ghobrial RM, Ferrari M, Grattoni A. J Control Release. 2013; 172(3):1011–1019. [PubMed: 24095805]

Ferrati S, Nicolov E, Bansal S, Zabre E, Geninatti T, Ziemys A, Hudson L, Ferrari M, Goodall R, Khera M, Palapattu G, Grattoni A. Adv Healthc Mater. (In press).

Fine D, Grattoni A, Hosali S, Ziemys A, De Rosa E, Gill J, Medema R, Hudson L, Kojic M, Milosevic M, Brousseau L III, Goodall R, Ferrari M, Liu X. Lab Chip. 2010; 10(22):3074–3083. [PubMed: 20697650]

Fine D, Grattoni A, Zabre E, Hussein F, Ferrari M, Liu X. Lab Chip. 2011; 11(15):2526–2534. [PubMed: 21677944]

Fine D, Grattoni A, Goodall R, Bansal SS, Chiappini C, Hosali S, van de Ven AL, Srinivasan S, Liu X, Godin B, Brousseau L 3rd, Yazdi IK, Fernandez-Moure J, Tasciotti E, Wu HJ, Hu Y, Klemm S, Ferrari M. Adv Healthc Mater. 2013; 2(5):632–666. [PubMed: 23584841]

Franks W, Schenker I, Schmutz P, Hierlemann A. IEEE Trans Biomed Eng. 2005; 52(7):1295–1302. [PubMed: 16041993]

Fu J, Schoch RB, Stevens AL, Tannenbaum SR, Han J. Nat Nanotechnol. 2007; 2(2):121–128. [PubMed: 18654231]

Geninatti T, Small E, Grattoni A. Meas Sci Technol. 2014; 25(2):027003.

Gossett DR, Weaver WM, Mach AJ, Hur SC, Tse HT, Lee W, Amini H, Di Carlo D. Anal Bioanal Chem. 2010; 397(8):3249–3267. [PubMed: 20419490]

Grattoni A, Fine D, Ziemys A, Gill J, Zabre E, Goodall R, Ferrari M. Curr Pharm Biotechnol. 2010; 11(4):343–365. [PubMed: 20199382]

Grattoni A, Fine D, Zabre E, Ziemys A, Gill J, Mackeyev Y, Cheney MA, Danila DC, Hosali S, Wilson LJ, Hussain F, Ferrari M. ACS Nano. 2011a; 5(12):9382–9391. [PubMed: 22032773]

Grattoni A, Gill J, Zabre E, Fine D, Hussain F, Ferrari M. Anal Chem. 2011b; 83(8):3096–3103. [PubMed: 21434670]

Han A, Wang O, Graff M, Mohanty SK, Edwards TL, Han KH, Bruno Frazier A. Lab Chip. 2003; 3(3):150–157. [PubMed: 15100766]

Humayun MS, de Juan E Jr, Weiland JD, Dagnelie G, Katona S, Greenberg R, Suzuki S. Vision Res. 1999; 39(15):2569–2576. [PubMed: 10396625]

Mukundan V, Pruitt BL. J Microelectromech Syst. 2009; 18(2):405–413. [PubMed: 20161046]

Nguyen B, Kassegne S. Microfluid Nanofluid. 2008; 5(3):383–393.

Pennisi CP, Sevcencu C, Dolatshahi-Pirouz A, Foss M, Hansen JL, Larsen AN, Zachar V, Besenbacher F, Yoshida K. Nanotechnology. 2009; 20(38):385103. [PubMed: 19713588]

Russell DBP, Thornton J. Digital Instruments AN46(Rev A 1). 2004

Sabek OM, Ferrati S, Fraga DW, Sih J, Zabre EV, Fine DH, Ferrari M, Gaber AO, Grattoni A. Lab Chip. 2013; 13(18):3675–3688. [PubMed: 23884326]

Sevcencu C, Dolatshahi-Pirouz A, Foss M, Lundsgaard Hansen J, Zachar V, Besenbacher F, Yoshida K. Artif Organs. 2007; 31(8):A9. No. 19.

Sih J, Bansal SS, Filippini S, Ferrati S, Raghuwansi K, Zabre E, Nicolov E, Fine D, Ferrari M, Palapattu G, Grattoni A. Anal Bioanal Chem. 2013; 405(5):1547–1557. [PubMed: 23090650]

Smolensky MH, Peppas NA. Adv Drug Deliv Rev. 2007; 59(9–10):828–851. [PubMed: 17884237]

Stieglitz T, Gross M. Sens Actuators B. 2002; 83(1–3):8–14.

Sun W, Zheng R, Chen X. J Power Sources. 2010; 195(20):7120–7125.

Tai C, Roppolo JR, de Groat WC. J Urol. 2004; 172(5 Pt 1):2069–2072. [PubMed: 15540791]

Taraballi F, Natalello A, Campione M, Villa O, Doglia SM, Paleari A, Gelain F. Front Neuroeng. 2010; 3:1. [PubMed: 20162033]

Tordoir JH, Scheffers I, Schmidli J, Savolainen H, Liebeskind U, Hansky B, Herold U, Irwin E, Kroon AA, de Leeuw P, Peters TK, Kieval R, Cody R. Eur J Vasc Endovasc Surg. 2007; 33(4):414–421. [PubMed: 17227715]

Turner N, Armitage M, Butler R, Ireland G. Cell Biol Int. 2004; 28(7):541–547. [PubMed: 15261162]

Vieu C, Carcenac F, Pépin A, Chen Y, Mejias M, Lebib A, Manin-Ferlazzo L, Couraud L, Launois H. Appl Surf Sci. 2000; 164(1–4):111–117.

Walczak R, Boiarski A, Cohen M, West T, Melnik K, Shapiro J, Sharma S, Ferrari M. Nano Biotechnology. 2005; 1(1):35–42.

Yeh LH, Xue S, Joo SW, Qian S, Hsu JP. J Phys Chem C. 2012; 116(6):4209–4216.

Yossifon G, Mushenheim P, Chang YC, Chang HC. Phys Rev E Stat Nonlin Soft Matter Phys. 2009; 79(4 Pt 2):046305. [PubMed: 19518331]

Youan BB. Adv Drug Deliv Rev. 2010; 62(9–10):898–903. [PubMed: 20438781]

Zhang M, Desai T, Ferrari M. Biomaterials. 1998; 19(10):953–960. [PubMed: 9690837]

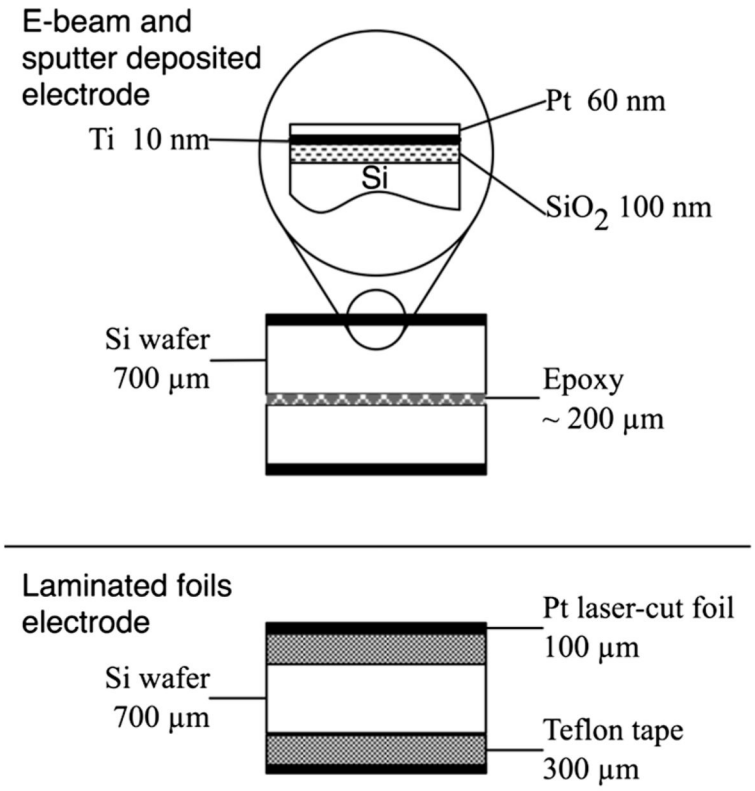

Fig. 1.
Electrodes/wafer sandwiches for e-beam deposited, sputter deposited, and foil electrodes

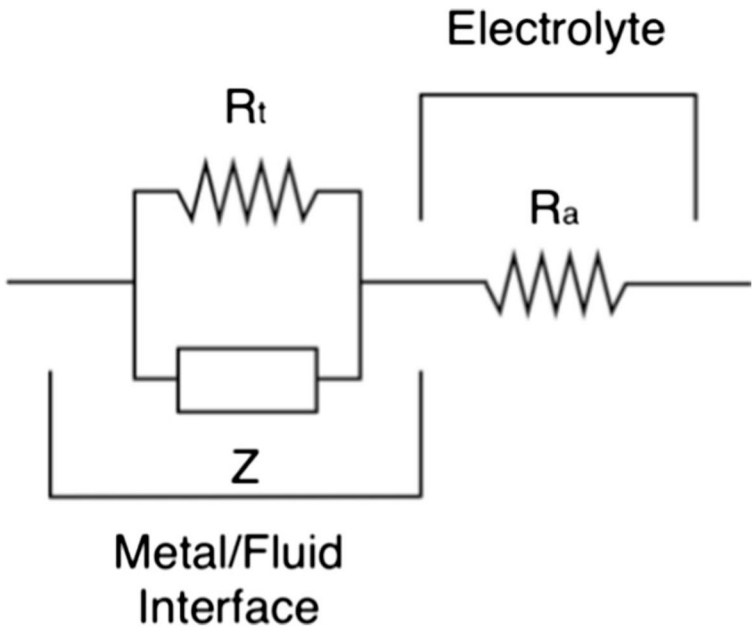

Fig. 2.
Equivalent circuit employed to model electrodes-electrolyte interface

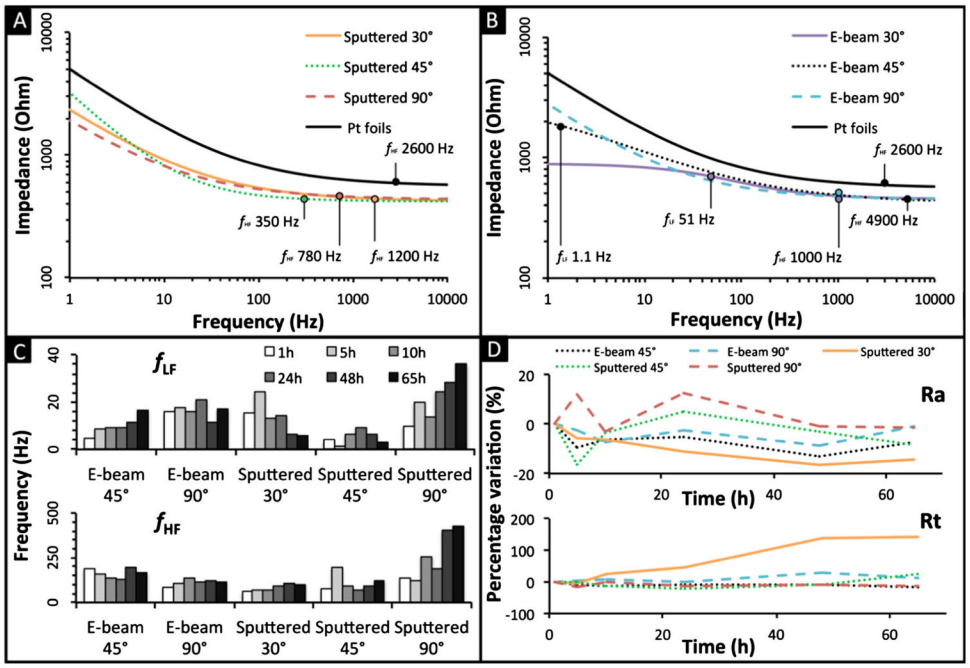

Fig. 3.

Impedance characterization of e-beam deposited Pt electrodes, Pt sputter deposited electrodes, and laminated Pt foils in PBS (**a** and **b**) and in cell culture (**c** and **d**). **a** Comparison of Impedance modulus of the sputter deposited Pt electrodes with laminated Pt foil in PBS solution; **b** Comparison of impedance modulus of the e-beam deposited Pt electrodes with laminated Pt foil in PBS solution; **c** variation of the separation between the LF with the MF domain due to the translation of the f_{LF}, and translation of the MF-HF regimes due to the f_{HF}, and **d** percentage variation of leak resistance R_t and the electrolyte resistance R_a in cell culture over time

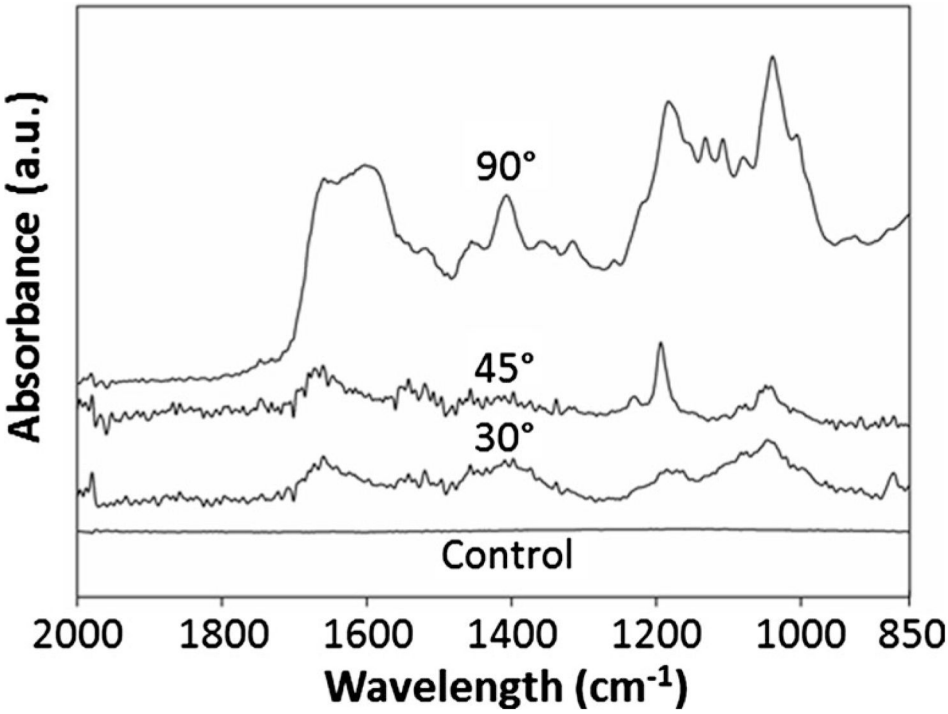

Fig. 4.

ATR-FTIR spectra of 30, 45 and 90° Pt sputtered electrode soaked in cell culture media, and 90° sputter Pt electrode employed has control soaked in MilliQ water

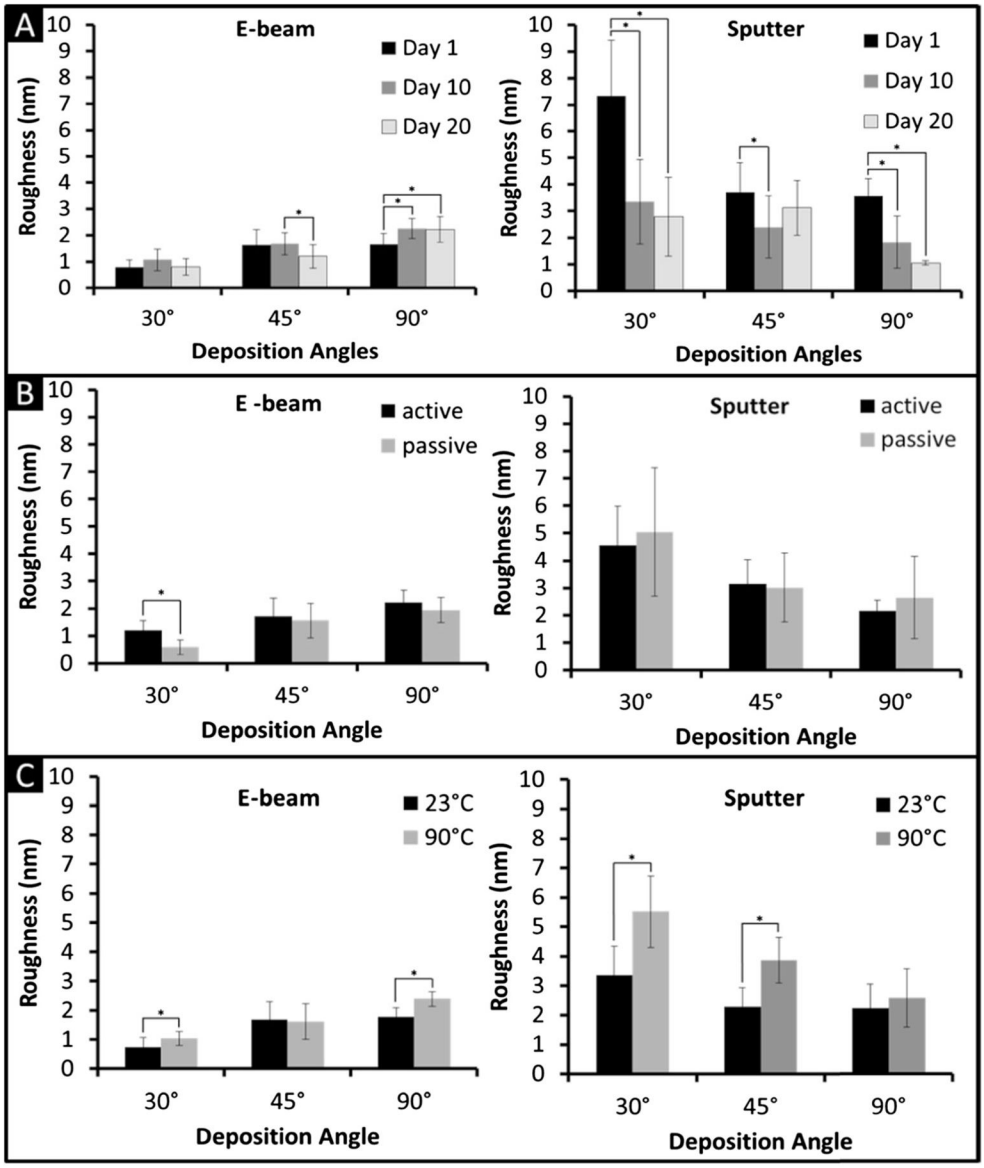

Fig. 5.

Degradation values. **a** degradation values over time, **b** degradation values under active (1.5 V) and passive (0 V) conditions, **c** degradation values under room temperature (23 °C) and accelerated conditions (90 °C). The asterisk (*) highlight a $P<0.05$

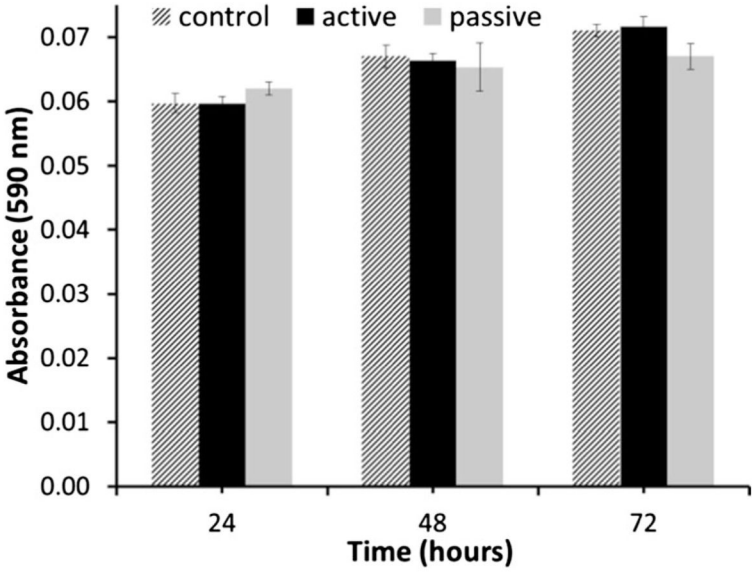

Fig. 6.
MTT proliferation assay results at 24, 48, and 72 h

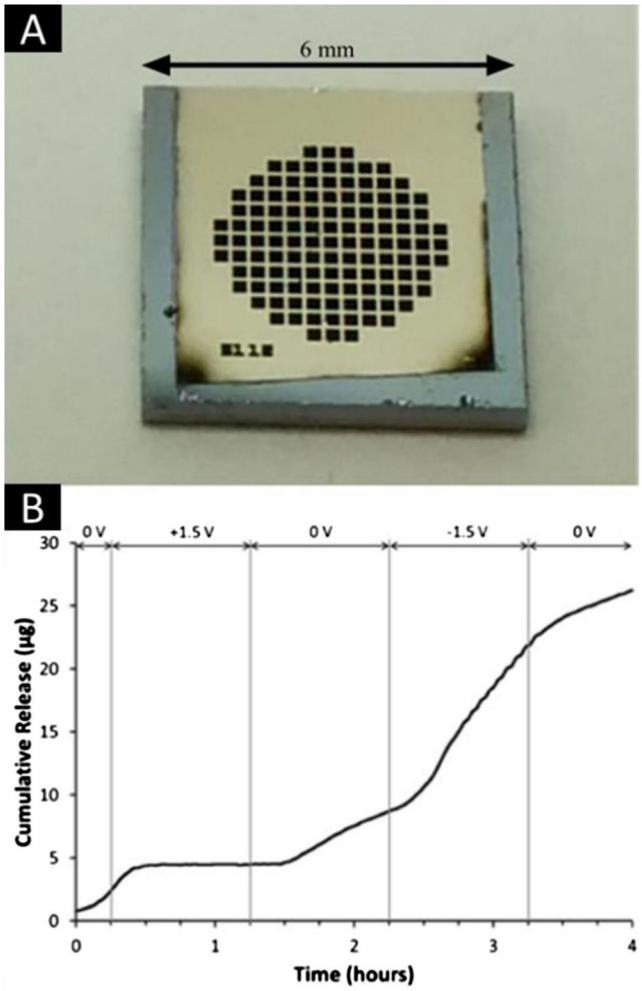

Fig. 7.

a Image of the Pt electrode e-beam deposited onto the 200 nm nanochannel membrane. **b** Modulation of dendritic fullerene 1 (DF-1) release

Table 1

Model parameters obtained by fitting the experimental data

	E-beam			Sputtered			Pt foils
	30°	**45°**	**90°**	**30°**	**45°**	**90°**	
R_a (Ω)	484.3	418.3	446.7	418.4	419.3	432.3	557.7
R_t (Ω)	$4.5\ 10^{2}$	2.83	$1.0\ 10^{5}$	$5.3\ 10^{4}$	$2.4\ 10^{5}$	$4.3\ 10^{4}$	$6.7\ 10^{4}$
$Q\left(\sqrt[n]{S}s\right)$	$6.0\ 10^{-7}$	$1.8\ 10^{-8}$	$2.3\ 10^{-7}$	$1.5\ 10^{-7}$	$2.8\ 10^{-6}$	$2.1\ 10^{-7}$	$5.2\ 10^{-8}$
n	0.72	0.50	0.58	0.55	0.73	0.55	0.57
f_{LF} (Hz)	51.600	1.134	$1.7\ 10^{-3}$	$2.9\ 10^{-3}$	$2.6\ 10^{-3}$	$2.5\ 10^{-3}$	$1.0\ 10^{-2}$
f_{HF}(Hz)	999.2	4880.4	1029.6	1238.1	345.4	784.8	2594.1

Table 2

Mean (n=3) surface roughness (R_{RMS}) for each experimental set up obtained by AFM

Roughness (nm)	30°				45°				90°			
	0 Volt		1.5 Volt		0 Volt		1.5 Volt		0 Volt		1.5 Volt	
	23 °C	90 °C	23 °C	90 °C	23 °C	90 °C	23 °C	90 °C	23 °C	90 °C	23 °C	90 °C
Day 1 (e-beam)	0.6 (±0.0)	0.6 (±0.0)	0.8 (±0.0)	1.2 (±0.0)	1.6 (±0.7)	1.3 (±0.0)	2.5 (±0.1)	1.5 (±0.4)	1.2 (±0.0)	2.1 (±0.2)	1.5 (±0.1)	2.3 (±0.5)
Day 10 (e-beam)	0.5 (±0.0)	1.3 (±0.3)	1.3 (±0.0)	1.3 (±0.1)	1.7 (±0.3)	1.6 (±0.5)	1.8 (±0.3)	1.6 (±0.7)	1.9 (±0.1)	2.5 (±0.1)	1.9 (±0.1)	2.7 (±0.2)
Day 20 (e-beam)	0.4 (±0.1)	0.8 (±0.0)	1.1 (±0.2)	1.0 (±0.0)	0.8 (±0.0)	1.9 (±0.1)	1.1 (±0.0)	1.1 (±0.1)	1.5 (±0.0)	2.4 (±0.2)	2.6 (±0.3)	2.4 (±0.1)
Day 1 (sputter)	4.8 (±1.5)	9.4 (±0.6)	5.6 (±0.2)	8.7 (±0.3)	2.7 (±0.3)	3.9 (±1.2)	3.0 (±0.0)	4.8 (±1.1)	5.4 (±1.7)	2.9 (±0.0)	3.2 (±0.3)	4.0 (±0.5)
Day 10 (sputter)	2.7 (±0.1)	5.5 (±0.4)	2.0 (±0.2)	3.2 (±1.6)	1.6 (±1.1)	3.6 (±0.2)	1.3 (±0.0)	3.2 (±0.4)	0.7 (±0.1)	3.9 (±0.5)	1.7 (±0.1)	1.7 (±0.6)
Day 20 (sputter)	1.4 (±0.3)	1.9 (±0.0)	3.6 (±1.7)	4.4 (±0.4)	1.9 (±0.1)	4.5 (±0.4)	2.9 (±0.3)	3.3 (±0.4)	1.0 (±0.1)	2.7 (±0.7)	1.3 (±0.3)	1.1 (±0.0)

Table 3

Mean (n=3) ICP-MS data of Pt in solution due to electrode degradation in PBS solution. Undetectable values are indicated as "–"

Degraded amount (ng/mm^2)	30°				45°				90°			
	0 Volt		1.5 Volt		0 Volt		1.5 Volt		0 Volt		1.5 Volt	
	23 °C	90 °C	23 °C	90 °C	23 °C	90 °C	23 °C	90 °C	23 °C	90 °C	23 °C	90 °C
Day 10 (e-beam)	–	–	–	7.4	11.9	7.1	9.3	2.2	0.2	0.4	0.2	0.4
Day 20 (e-beam)	–	–	–	–	6.2	6.4	–	3.8	0.2	0.5	0.2	0.5
Day 10 (spuntter)	11.6	28.0	14.3	5.4	7.3	8.9	5.0	8.9	8.5	7.3	13.1	2.7
Day 20 (spuntter)	19.7	100.4	–	4.2	7.3	10.8	3.5	3.1	11.2	10.0	20.5	6.2